



CFD solutions for magnetohydrodynamic natural convection over horizontal and vertical surfaces



Kaustav Pradhan *, Abhijit Guha

Mechanical Engineering Department, Indian Institute of Technology Kharagpur, Kharagpur 721302, India

ARTICLE INFO

Article history:

Received 18 March 2016

Received in revised form 7 March 2017

Accepted 29 March 2017

Available online 02 April 2017

Keywords:

MHD

Natural convection

Non-similarity

CFD

Time-marching

ABSTRACT

This paper investigates the effects of a magnetic field on the natural convective boundary layer flow of an electrically conducting fluid adjacent to horizontal as well as vertical surfaces. This has allowed us to establish overall similarities and several subtle differences between the two cases. Previously published studies concentrated on obtaining self-similar solutions at the cost of assuming very restrictive variation of the magnetic field along the surface. In the present work, a numerical model and an in-house computer program have been developed to solve directly the non-linear boundary layer equations which can accommodate any arbitrary variation of the magnetic field. Special emphasis is given to the case of uniform magnetic field which perhaps represents the most practical case and which cannot be solved by the similarity theory. Computations show that the Nusselt number and the skin-friction coefficient decrease as the magnetic field increases. It is shown that the detailed characteristics of the velocity profiles and the values of Nusselt number and skin-friction coefficient for the case of a magnetic field which admits similarity are significantly different from those when a uniform magnetic field is applied, thus showing the importance of the present model.

© 2017 Elsevier B.V. All rights reserved.

1. Introduction

Magnetohydrodynamics (MHD) is the study of the interaction between a moving fluid and a magnetic field. When a magnetic field is applied perpendicular to the main flow direction, the magnetic lines offer a resistance to the flow and cause a retardation [1]. The study of magnetohydrodynamic natural convection has gained much importance due to its application in the field of geophysical engineering, enhanced oil recovery and nuclear sciences [2]. The flow control achieved by the application of a magnetic field is of particular use in metallurgical and polymer processing industries [3]. Relevant examples of Newtonian fluids, for which a magnetic field may have an effect, include liquid metals, ionized gases, electrolytic solutions and certain water-based nanofluids.

The laminar natural convection of electrically conducting fluids past a heated vertical surface in the presence of a magnetic field has been studied by many researchers [4–7]. Riley [4] used a method of “matching ‘outer’ and ‘inner’ solutions in the moving layer of fluid” in his studies for strong magnetic fields. Lykoudis [6] obtained similarity solutions for a specific variation of the magnetic field. Sparrow and Cess [7] found that the application of a magnetic field significantly affects the free convection heat transfer to liquid metals. Self-similar

solutions for magnetohydrodynamic natural convection past a vertical plate exist only when the strength of the magnetic field varies as the inverse of the fourth root of the distance from the leading edge [5,6]. In spite of the existence of numerous studies on the magnetohydrodynamic natural convection over a vertical plate, the effect of a uniform magnetic field (which is of greater physical significance but does not admit self-similar solutions) has not been investigated thoroughly.

Natural convective boundary layer flow over a horizontal surface is quite different from its counterpart on a vertical surface and the flow is set up indirectly by the buoyancy force acting normal to the surface. This is why Schlichting and Gersten referred to this as “indirect natural convection” [8]. Theoretical and numerical studies of this type of flow for various types of fluids and boundary conditions may be found in [9–15]. Natural convection over a heated horizontal surface under the influence of a vertical magnetic field has been analysed by Gupta [16] using the momentum-integral method. Gupta [16] considered self-similar solutions for two cases: (i) the magnetic field varying as the inverse of the two-fifth power of the distance along the plate (from the leading edge) when the surface temperature is constant, and, (ii) the temperature difference varying as the square of the distance and the boundary layer thickness being held constant for a uniform magnetic field. Similar studies using the integral technique have been performed by Singh [17,18] and Singh and Cremers [19]. Samanta and Guha [20] performed a similarity analysis for the magnetohydrodynamic natural convection over an isothermal horizontal plate, assuming the magnetic field to vary as the inverse of the two-fifth power of the distance along

* Corresponding author.

E-mail addresses: kaustav.pradhan@mech.iitkgp.ernet.in (K. Pradhan), a.guha@mech.iitkgp.ernet.in (A. Guha).

Nomenclature

B_0	strength of a uniform magnetic field
c_f	skin-friction coefficient
c_f^*	reduced skin-friction coefficient
Gr_L	Grashof number defined as $g\beta(T_w - T_\infty)L^3/\nu^2$
Gr_x	local Grashof number defined as $g\beta(T_w - T_\infty)x^3/\nu^2$
g	acceleration due to gravity
k	thermal conductivity of the fluid
L	reference length
M	magnetic interaction parameter
M_0	magnetic interaction parameter corresponding to B_0
Nu	Nusselt number
Nu^*	reduced Nusselt number
ΔNu^*	relative difference in Nu^* , defined in Eq. (33)
Pr	Prandtl number
p	static pressure
\bar{p}	dimensionless static pressure
q_w	surface heat flux
r	successive ratio for grid spacing
T	temperature of the fluid
u, v	velocity components along and normal to the surface
\bar{u}, \bar{v}	dimensionless velocity components
u_0	reference velocity
\vec{V}	fluid velocity vector
x, y	distance along and normal to the surface
\bar{x}, \bar{y}	dimensionless variables for x and y

Greek symbols

α	thermal diffusivity of the fluid
β	volume coefficient of thermal expansion
δ	defined as $LG\bar{r}_L^{-1/5}$ for horizontal case and $LG\bar{r}_L^{-1/4}$ for vertical case
η	similarity variable
θ	dimensionless temperature
λ	index in power-law variation of magnetic field (Eq. (30))
μ	dynamic viscosity
ρ	fluid density
σ	electrical conductivity
τ_w	wall shear stress
ν	kinematic viscosity

Subscripts

w	value of a variable at the surface
∞	ambient condition

the plate (from the leading edge). The authors of ref. [19] recognized that the effect of a uniform magnetic field on the natural convective flow is of more physical interest than the relations stated above. Their short paper [19] used an integral formulation, complex co-ordinate transformation, and, in the end, a numerical integration process to obtain results that are valid only for fluids with very low Prandtl number ($Pr = 1/40$).

In the present work, the power of computational fluid dynamics is invoked to reveal the details of magnetohydrodynamic natural convection flow field and heat transfer on isothermally heated horizontal or vertical surfaces. The effects of different variations of the applied magnetic field are investigated thoroughly. The developed computer programs are able to accommodate any arbitrary variation of the magnetic field, thus eliminating the characteristic limitation of all previous studies seeking similarity solutions. The uniform magnetic field perhaps represents the most practical situation and hence much emphasis

is put on the natural convective flow field and heat transfer under the application of a uniform field. We have studied the effect of the magnetic field and Prandtl number on the heat transfer and the skin friction, and on the spatial evolution of the boundary layer.

2. Mathematical formulation

The mutual interaction of the flow of a conducting fluid and an applied magnetic field gives rise to an additional body force on the fluid called the Lorentz force. The relative motion of the conducting fluid and the magnetic field sets up an electric current. This induced current, in turn, gives rise to an induced magnetic field which adds to the applied magnetic field and produces an effect such that the fluid appears to drag the magnetic field lines along with it. Therefore, there exists, in general, a two-way coupling between the magnetic field and the velocity field of the conducting fluid. The total magnetic field (applied plus induced) interacts with the induced current to give rise to the Lorentz force which is given by the relation [1]:

$$\vec{F} = \vec{J} \times \vec{B} \quad (1)$$

where $\vec{J} = \sigma(\vec{E} + \vec{V} \times \vec{B})$ is the electric current density, σ is the electrical conductivity of the fluid, \vec{E} is an external electric field, \vec{V} is the velocity of the fluid and \vec{B} is the magnetic field.

The importance of the induced magnetic field is assessed by the magnitude of the magnetic Reynolds number Re_m , defined as,

$$Re_m = \mu_0 \sigma u L \quad (2)$$

where μ_0 is the magnetic permeability, u a component of the fluid velocity and L is a reference length. For most laboratory experiments or industrial processes involving liquid metals, $\mu_0 \sigma \sim 1 \text{ s/m}^2$ [1], $L \sim 0.1 \text{ m}$ [1] and for natural convection $u \sim 0.1 \text{ m/s}$. This gives $Re_m \sim 0.01$. Under these conditions, it is possible to neglect the induced magnetic field as compared to the applied magnetic field [21]. For the present work, it is assumed that the value of Re_m is very small, which means that the induced electric current is unable to appreciably distort the applied magnetic field. This leads to a situation where the coupling between the magnetic field and the velocity field becomes one way; \vec{B} affects the velocity field \vec{V} through the Lorentz force, but \vec{V} does not substantially alter the applied magnetic field \vec{B} . It is also assumed that there is no external electrical field ($\vec{E} = 0$). The Lorentz force can then be simplified as

$$F_x = -\sigma B^2 u \quad (3)$$

where B is the strength of a magnetic field applied perpendicular to the u component of fluid velocity.

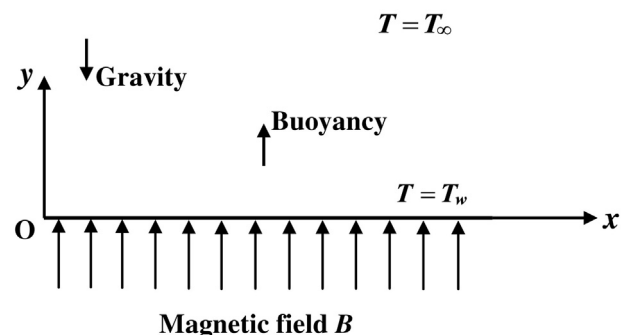


Fig. 1. Physical model and coordinate system for the horizontal surface.

2.1. Formulation for horizontal surface

Consider a horizontal surface maintained at a temperature T_w . The quiescent ambient fluid is at a temperature $T_\infty (T_\infty < T_w)$ and pressure p_∞ . The x -axis is taken along the horizontal surface while the y -axis is taken normal to the surface with the leading edge at the origin. A vertical magnetic field B is applied as shown in Fig. 1.

The governing equations for natural convection over a horizontal surface, in the presence of a vertical magnetic field, may be found in ref. [20]. These equations, in non-dimensional form, are:

$$\frac{\partial \bar{u}}{\partial \bar{x}} + \frac{\partial \bar{v}}{\partial \bar{y}} = 0 \tag{4}$$

$$\bar{u} \frac{\partial \bar{u}}{\partial \bar{x}} + \bar{v} \frac{\partial \bar{u}}{\partial \bar{y}} = -\frac{\partial \bar{p}}{\partial \bar{x}} + \frac{\partial^2 \bar{u}}{\partial \bar{y}^2} - M\bar{u} \tag{5}$$

$$0 = -\frac{\partial \bar{p}}{\partial \bar{y}} + \theta \tag{6}$$

$$\bar{u} \frac{\partial \theta}{\partial \bar{x}} + \bar{v} \frac{\partial \theta}{\partial \bar{y}} = \frac{1}{Pr} \frac{\partial^2 \theta}{\partial \bar{y}^2} \tag{7}$$

The non-dimensional variables appearing in the above equations are obtained by an order of magnitude analysis [11] and are defined as follows:

$$\left. \begin{aligned} \bar{x} &= \frac{x}{L}, \\ \bar{y} &= \frac{y}{L} (Gr_L)^{1/5}, \\ \bar{u} &= \frac{u}{u_0}, \\ \bar{v} &= \frac{v}{u_0} (Gr_L)^{1/5}, \\ \bar{p} &= \frac{p - p_\infty}{\rho u_0^2}, \\ \theta &= \frac{T - T_\infty}{T_w - T_\infty}. \end{aligned} \right\} \tag{8}$$

where L is a reference length and u_0 is the reference velocity given by ref. [11]

$$u_0 = \frac{v}{L} (Gr_L)^{2/5} \tag{9}$$

The dimensionless parameters Grashof number Gr_L , Prandtl number Pr and the magnetic interaction parameter M are defined as follows:

$$\left. \begin{aligned} Gr_L &= \frac{g\beta(T_w - T_\infty)L^3}{\nu^2}, \\ Pr &= \frac{\nu}{\alpha}, \\ M &= \frac{\sigma B^2 L}{\rho u_0} = \frac{\sigma B^2 L^2}{\mu Gr_L^{2/5}}. \end{aligned} \right\} \tag{10}$$

The interaction parameter defined above is a ratio of the square of the Hartmann number ($Ha \equiv BL\sqrt{\sigma/\mu}$) to the flow Reynolds number ($Re \equiv u_0 L/\nu$).

The solution to the non-dimensional Eqs. (4)–(7) depends only on the values of two parameters: Pr and M . The Grashof number does not appear explicitly in the non-dimensional governing Eqs. (4)–(7). When there is no magnetic field, (i.e. $B = 0$, and, therefore $M = 0$), the solution of Eqs. (4)–(7) depends only on Pr , and then the reference length L is directly related to the adopted value of Grashof number through the equation $Gr_L = g\beta(T_w - T_\infty)L^3/\nu^2$. For non-zero values of M , however, Eq. (10) shows that the parameter M and L are related such that $M = \Psi L^{4/5}$, where $\Psi = \sigma B^2 / [\mu \{g\beta(T_w - T_\infty)/\nu^2\}^{2/5}]$. For given

values of fluid properties, magnetic field, temperature difference and acceleration due to gravity, L is then implicitly parametrized through M .

The non-dimensional variable \bar{y} (defined in Eq. (8)) is obtained from the dimensional variable y by global scaling with δ deduced in an order of magnitude analysis [11], i.e. $\delta \sim LGr_L^{-1/5}$. Since it has already been established in the literature that self-similar solutions do not exist for any arbitrary variation of the magnetic field, it is imperative to solve a system of partial differential equations. We have therefore avoided the complex transformations [6,7] associated with using the local boundary layer thickness as the scaling factor for the y variable.

The boundary conditions for the governing equations in non-dimensional form are:

$$\text{at } \bar{y} = 0, \text{ for all } \bar{x}, \quad \bar{u} = \bar{v} = 0, \theta = 1 \tag{11}$$

$$\text{as } \bar{y} \rightarrow \infty, \text{ for all } \bar{x}, \quad \bar{u} \rightarrow 0, \theta \rightarrow 0, \bar{p} \rightarrow 0 \tag{12}$$

$$\text{at } \bar{x} = 0, \text{ for } \bar{y} > 0, \quad \bar{u} = 0, \theta = 0, \bar{p} = 0. \tag{13}$$

The boundary condition in Eq. (13) is based on the assumption that the boundary layer originates at the leading edge [22].

2.2. Formulation for vertical surface

Consider a heated vertical surface maintained at a temperature T_w . The x -axis is taken along the surface while the y -axis is taken normal to it with the leading edge at the origin. A horizontal magnetic field B is applied as shown in Fig. 2.

The governing equations for natural convection past a vertical surface, in the presence of a horizontal magnetic field, may be found in ref. [7]. These equations, in non-dimensional form, are:

$$\frac{\partial \bar{u}}{\partial \bar{x}} + \frac{\partial \bar{v}}{\partial \bar{y}} = 0 \tag{14}$$

$$\bar{u} \frac{\partial \bar{u}}{\partial \bar{x}} + \bar{v} \frac{\partial \bar{u}}{\partial \bar{y}} = \theta + \frac{\partial^2 \bar{u}}{\partial \bar{y}^2} - M\bar{u} \tag{15}$$

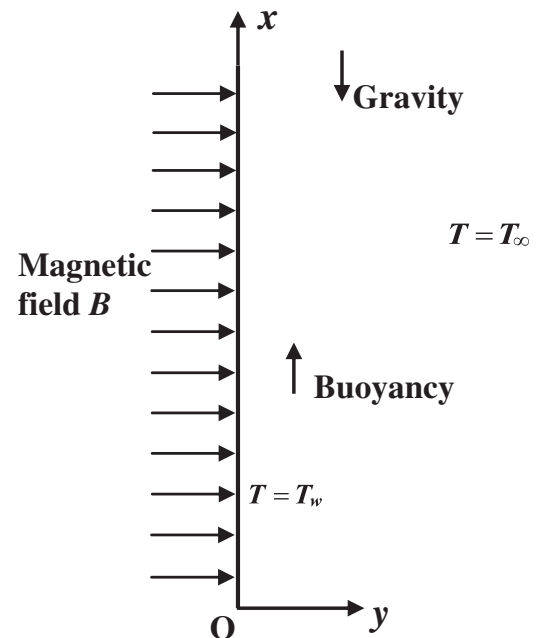


Fig. 2. Physical model and coordinate system for the vertical surface.

$$\bar{u} \frac{\partial \theta}{\partial \bar{x}} + \bar{v} \frac{\partial \theta}{\partial \bar{y}} = \frac{1}{Pr} \frac{\partial^2 \theta}{\partial \bar{y}^2} \quad (16)$$

The non-dimensional variables appearing in the above equations are obtained by an order of magnitude analysis and are defined as follows:

$$\left. \begin{aligned} \bar{x} &= \frac{x}{L}, \\ \bar{y} &= \frac{y}{L} (Gr_L)^{1/4}, \\ \bar{u} &= \frac{u}{u_0}, \\ \bar{v} &= \frac{v}{u_0} (Gr_L)^{1/4}, \\ \theta &= \frac{T - T_\infty}{T_w - T_\infty} \end{aligned} \right\} \quad (17)$$

where L is a reference length and u_0 is the reference velocity given by ref. [23]

$$u_0 = \frac{v}{L} (Gr_L)^{1/2} \quad (18)$$

The non-dimensional variable \bar{y} (defined in Eq. (17)) is obtained from the dimensional variable y by global scaling with δ deduced in an order of magnitude analysis, i.e. $\delta \sim L Gr_L^{-1/4}$.

The magnetic interaction parameter M appearing in Eq. (15) is different from that given in Eq. (10) due to the different reference velocities used in the horizontal and vertical cases. The expression for M in case of the vertical surface is given by,

$$M = \frac{\sigma B^2 L}{\rho u_0} = \frac{\sigma B^2 L^2}{\mu Gr_L^{1/2}} \quad (19)$$

For non-zero values of M , Eq. (19) shows that the parameter M and L are related such that $M = \Psi L^{1/2}$, where $\Psi = \sigma B^2 / [\mu \{g\beta(T_w - T_\infty)/v^2\}^{1/2}]$. For given values of fluid properties, magnetic field, temperature difference and acceleration due to gravity, L is then implicitly parametrized through M .

The boundary conditions for the governing equations in non-dimensional form are:

$$\text{at } \bar{y} = 0, \text{ for all } \bar{x}, \quad \bar{u} = \bar{v} = 0, \theta = 1 \quad (20)$$

$$\text{as } \bar{y} \rightarrow \infty, \text{ for all } \bar{x}, \quad \bar{u} \rightarrow 0, \theta \rightarrow 0 \quad (21)$$

$$\text{at } \bar{x} = 0, \text{ for } \bar{y} > 0, \quad \bar{u} = 0, \theta = 0. \quad (22)$$

The boundary condition in Eq. (22) is based on the assumption that the boundary layer originates at the leading edge [24].

2.3. Heat transfer and skin-friction

The Nusselt number Nu and the skin-friction coefficient c_f are important parameters in natural convective flow over flat plates.

2.3.1. For a horizontal surface

Using Eqs. (8) and (9), the Nusselt number and the skin-friction coefficient can be derived as follows:

$$Nu = \frac{q_w L}{k(T_w - T_\infty)} = \frac{-k(\partial T / \partial y)_{y=0} L}{k(T_w - T_\infty)} = -(Gr_L)^{1/5} \left(\frac{\partial \theta}{\partial \bar{y}} \right)_{\bar{y}=0} \quad (23)$$

$$c_f = \frac{\tau_w}{\rho u_0^2 / 2} = \frac{\mu(\partial u / \partial y)_{y=0}}{\rho u_0^2 / 2} = 2(Gr_L)^{-1/5} \left(\frac{\partial \bar{u}}{\partial \bar{y}} \right)_{\bar{y}=0} \quad (24)$$

A reduced Nusselt number Nu^* and a reduced skin-friction coefficient c_f^* are defined as,

$$Nu^* = \frac{Nu}{(Gr_L)^{1/5}} = - \left(\frac{\partial \theta}{\partial \bar{y}} \right)_{\bar{y}=0} \quad (25)$$

$$c_f^* = \frac{c_f}{2(Gr_L)^{-1/5}} = \left(\frac{\partial \bar{u}}{\partial \bar{y}} \right)_{\bar{y}=0} \quad (26)$$

2.3.2. For a vertical surface

Similarly, using Eqs. (17) and (18), the reduced Nusselt number Nu^* and the reduced skin-friction coefficient c_f^* for the natural convection along a vertical surface are given by the following expressions:

$$Nu^* = \frac{Nu}{(Gr_L)^{1/4}} = - \left(\frac{\partial \theta}{\partial \bar{y}} \right)_{\bar{y}=0} \quad (27)$$

$$c_f^* = \frac{c_f}{2(Gr_L)^{-1/4}} = \left(\frac{\partial \bar{u}}{\partial \bar{y}} \right)_{\bar{y}=0} \quad (28)$$

2.4. Magnetic interaction parameter for power-law variation in magnetic field

Previous researchers have shown that self-similar solutions exist only when the applied magnetic field B is proportional to $x^{-2/5}$ in the case of a horizontal surface [20] and $x^{-1/4}$ in the case of a vertical surface [6]. In analogy to similarity theory, a power-law variation of the magnetic field is assumed here:

$$B = B_0 \bar{x}^\lambda \quad (29)$$

Then the magnetic interaction parameter in Eqs. (5) and (15) is given by

$$M = \frac{\sigma B_0^2 L}{\rho u_0} \bar{x}^{2\lambda} = M_0 \bar{x}^{2\lambda} \quad (30)$$

The particular values of λ , viz. $\lambda = -2/5$ and $\lambda = -1/4$, represent the cases required by the similarity theories as described above. The in-house computer programs developed for the present work can thus accommodate an arbitrary variation of the magnetic field.

In an engineering application, the case of a uniform magnetic field of strength B_0 seems to be the most relevant. The present computer models are able to simulate this situation since it corresponds to $\lambda = 0$ in Eqs. (29) and (30). The existing similarity theories, on the other hand, are only valid for $\lambda = -2/5$ for horizontal case and $\lambda = -1/4$ for vertical case, and, are thus very restrictive in their scope.

3. Method of solution

Two computer programs are developed using the finite difference method to solve the equation system (4)–(7) subject to the boundary conditions (11)–(13) for the horizontal surface, and, the equation system (14)–(16) subject to the boundary conditions (20)–(22) for the vertical surface. The present computer programs are based on that developed for non-Newtonian fluids described in [12].

3.1. Numerical technique

For the present work, we have adopted a time-marching technique [25–27] in which the final steady state is obtained as the limiting converged solution of an unsteady process. For this purpose, appropriate unsteady terms involving $\partial \bar{u} / \partial t$ and $\partial \theta / \partial t$ are introduced in the \bar{x} -

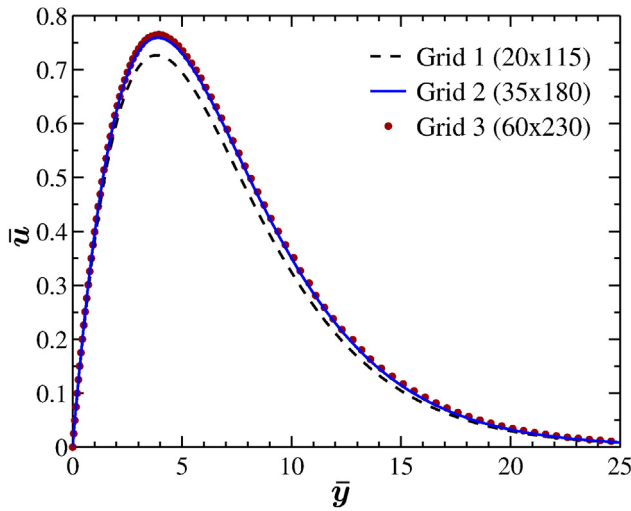


Fig. 3. Results of the grid independence test performed for three different grids in the case of a horizontal surface at $\bar{x} = 10$ with $M_0 = 1$, $\lambda = -2/5$ and $Pr = 0.7$. [The \bar{y} axis is shown here up to a value of 25 for clarity of the graphs, the maximum value used in the computations is greater so as to ensure \bar{u} asymptotically approaches zero.]

momentum equation and energy equation respectively. The time-marching technique begins with an initial specification of all the variables in the flow field, and then, as the name implies, marches forward in time until the solution converges (a convergence criterion of 10^{-8} has been used here). The selected time-marching scheme is explicit in nature, and, this imposes a restriction on the maximum permissible size of the time-step which depends on the minimum size of the spatial grid used.

This paper concentrates on laminar ($Gr_x \leq 10^9$ for vertical surfaces and $Gr_x \leq 10^6$ for horizontal surfaces [28]) natural convective boundary layers and instabilities of physical origin are not expected in the laminar regime. There may, however, be several sources of convective numerical instability in the computational solution process since the fluid dynamic equations are non-linear in nature, and this makes the computations challenging [12]. Moreover, the solution process for a horizontal surface suffers from an additional challenge (as compared to that for a vertical surface) since the v -velocity changes sign inside the boundary layer [12]. As we are interested only in the steady solution, and not on its unsteady development, under-relaxation factors are used in the present numerical scheme with values chosen from experience such that numerical instabilities are avoided but CPU time does not increase excessively.

A rectangular two-dimensional computational domain of size \bar{x}_{max} in the \bar{x} -direction and \bar{y}_{max} in the \bar{y} -direction is used for both the horizontal and the vertical cases. A grid of size $(m \times n)$ indicates that there are $m + 1$ and $n + 1$ grid points respectively along the \bar{x} and \bar{y} axes. As an example, Grid 1 (20×115) means that there are 21 grid points along the \bar{x} -direction and 116 grid points along the \bar{y} -direction. A uniform grid spacing is used along the \bar{x} direction while a non-uniform grid spacing is used along the \bar{y} direction such that the spacing ($\Delta\bar{y}$) is progressively increased, following a geometric progression, as one moves away from the solid surface.

3.2. Grid independence test

A comprehensive grid independence test has been performed at each value of the Prandtl number to determine the optimum choice of the two-dimensional grid. An example of grid independence test for the case of $M_0 = 1$, $\lambda = -2/5$ and $\bar{x}_{max} = 10$ at $Pr = 0.7$ is shown in Fig. 3 where results for three grid arrangements - Grid 1 (20×115), Grid 2 (35×180) and Grid 3 (60×230) - are displayed. The Nusselt number Nu and skin-friction c_f (both defined only at $\bar{y} = 0$) are the two most important (or practically useful) variables. However, our experience showed that even when the values of Nu and c_f have converged with sufficient accuracy, the \bar{u} -velocity profile, particularly its solution in the tail, may continue further to evolve with grid refinement. Experience also showed that the \bar{u} -velocity is the most sensitive to grid structure among the flow variables \bar{u} , \bar{v} , θ and \bar{p} . Accordingly, the \bar{u} -velocity profiles are displayed in Fig. 3 as the most stringent test of grid independence. It is observed that the \bar{u} -velocity profile obtained by using Grid 2 and Grid 3 are almost identical.

The values of Nusselt number and skin friction coefficient depend strongly on the grid structure, and particularly on the distance of the first computational grid point from the solid surface ($\Delta\bar{y}_1$). For Grid 2 (35×180), three values of $\Delta\bar{y}_1$ are tested, viz. 0.01, 0.05 and 0.07. Considering the significant increase in computational times (due to the use of explicit scheme) and the relatively small improvements in the results, achieved by using successively decreasing values of $\Delta\bar{y}_1$, the optimum value of $\Delta\bar{y}_1$ is chosen as 0.05 for all subsequent computations. Hence, Grid 2 is used for all subsequent computations with $\bar{x}_{max} = 10$ and $Pr = 0.7$. It is important to realize that the value of $\Delta\bar{y}_1 = 0.05$ should not be interpreted as that there are only about 20 grid points within the boundary layer. This is so because the δ used in the similarity theory is not an exact measure of the physical thickness of the boundary layer. An inspection of the figures given later shows that, for $M_0 = 1$ and $\bar{x} = 5$, the value of \bar{y} (where $\bar{y} = y/\delta$) is approximately 25 at the edge of the boundary layer at $Pr = 0.7$ and is approximately 100 at the edge of the boundary layer at $Pr = 0.01$. Thus, $\Delta\bar{y}_1 = 0.05$ actually provides many grid points within the boundary layer and ensures the demonstrated accuracy of the example computations presented here.

Other than the size of the first computational cell ($\Delta\bar{y}_1$), another important variable is the size of the overall computational domain. The value of \bar{y}_{max} must be carefully selected to ensure that the pressure, temperature and velocities reach asymptotically their respective values at $\bar{y} \rightarrow \infty$. This is done by selecting the value of \bar{y}_{max} to be greater than the thickness of the boundary layer at \bar{x}_{max} . (A quantitative measure of the boundary layer thickness is defined as that value of \bar{y} at which flow variables reach to within 1% of their values in the ambient fluid and the relative changes in flow variables asymptotically reach a small magnitude ($\leq 10^{-4}$)). It is found from extensive computations that \bar{y}_{max} must be increased as \bar{x}_{max} increases or Pr decreases. As an example, for $\bar{x}_{max} = 5$ and $Pr = 0.01$, a value of $\bar{y}_{max} = 100$ is used. For the same Prandtl number, when $\bar{x}_{max} = 10$, a value of $\bar{y}_{max} = 200$ is used. Keeping the value of \bar{x}_{max} fixed at 10, a value of $\bar{y}_{max} = 60$ is used for $Pr = 0.7$ as compared to $\bar{y}_{max} = 200$ for $Pr = 0.01$. Consequently, a separate grid independence test is required for the low Prandtl number case, where the number of points along the \bar{y} direction must be increased (while keeping $\Delta\bar{y}_1$ at its optimum value) so as to increase the size of the computational

Table 1

Temperature and velocity gradients at the wall for natural convection over an isothermal horizontal surface ($\eta = \bar{y}/\bar{x}^{2/5}$, $\theta'(0) = d\theta/d\eta|_{\eta=0}$, $f''(0) = d^2f/d\eta^2|_{\eta=0}$).

	Present work		Similarity solution [20]		Similarity solution [10]	
	$\theta'(0)$	$f''(0)$	$\theta'(0)$	$f''(0)$	$\theta'(0)$	$f''(0)$
$Pr = 0.7, M_0 = 0$	0.3593	0.9835	0.3547	0.9888	-	-
$Pr = 0.7, M_0 = 1, \lambda = -2/5$	0.2985	0.7574	0.2934	0.7560	-	-
$Pr = 0.72, M_0 = 0$	0.3633	0.9731	-	-	0.3591	0.9799
$Pr = 0.01, M_0 = 0$	0.0875	4.4624	0.0863	4.4645	-	-
$Pr = 0.01, M_0 = 1, \lambda = -2/5$	0.0792	3.2894	0.0755	3.2911	-	-

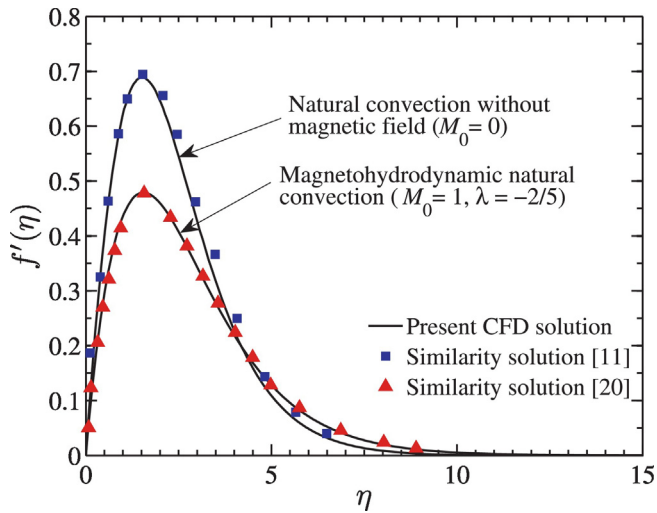


Fig. 4. Variation of the similarity variable representing the dimensionless u -velocity over a horizontal surface for $Pr = 0.7$ obtained by post-processing the present CFD solutions, and its comparison with the prediction of similarity theory ($\eta = \bar{y}/\bar{x}^{2/5}$, $f'(\eta) = df/d\eta = \bar{u}/\bar{x}^{1/5}$).

domain normal to the surface. The computational time is significantly increased due to this increase in the number of computational points in the \bar{y} direction. Three grid arrangements - Grid 4 (20×200), Grid 5 (35×260) and Grid 6 (60×330) are used to establish the grid independence of the solution at $Pr = 0.01$. Keeping in mind the level of accuracy achieved and the time required for computations, Grid 5 is selected for performing all sample calculations at $Pr = 0.01$ in the case of horizontal surfaces.

In order to maintain the optimum grid structure (determined by the grid independence test), the number of grid points along the \bar{x} -direction is increased as \bar{x}_{\max} increases. For example, while 36 grid points have been used along the \bar{x} -direction for $\bar{x}_{\max} = 10$, 141 grid points have been used in the \bar{x} -direction for $\bar{x}_{\max} = 40$.

After performing a similar grid independence test for the vertical surface, a (30×180) grid with $\Delta\bar{y}_1 = 0.05$ is chosen for all sample calculations at $Pr = 0.72$ and $\bar{x}_{\max} = 10$, and, a (30×320) grid with $\Delta\bar{y}_1 = 0.05$ is chosen for sample calculations at $Pr = 0.01$ and $\bar{x}_{\max} = 10$. The details of the grid independence test for the vertical case has not been included here for brevity.

3.3. Validation

The CFD method obviously does not use similarity variables. Thus the CFD results are post-processed and cast into the similarity variable form to enable a direct comparison with the predictions of previous similarity analyses. Table 1 gives a comparison of $\theta'(0)$ and $f''(0)$ (both variables arise in similarity theory, and have been defined in the table caption) calculated by the present technique and those existing in the literature for the case of a horizontal surface. Fig. 4 shows a comparison of the similarity variable for the u -velocity

obtained by previous researchers [11,20] with that obtained by the present computer program. Table 2 gives a comparison of $\theta'(0)$ and $f''(0)$ calculated by the present technique and those existing in the literature for the case of a vertical surface. The excellent matching of the present results with those in the literature validates the in-house computer programs developed and lends confidence to the new results generated.

4. Results and discussion

The effect of the variation of the applied magnetic field on the natural convective flow is thoroughly investigated. As mentioned in Section 2.4, power-law variation in the magnetic interaction parameter ($M = M_0\bar{x}^{2\lambda}$) is assumed in analogy with the practice followed for the similarity theory. The case of uniform magnetic field is represented by $M = M_0\neq f(\bar{x})$, i.e. M is fixed at all \bar{x} -locations in a single CFD simulation but different values of M_0 are ascribed for different CFD simulations.

An important application of magnetohydrodynamics arises in metallurgical processes involving the flow of liquid metals. Ionized air and particular water-based nanofluids or electrolytic solutions may have significant electrical conductivity such that the effect of an applied magnetic field on the flow of such fluids is important. However, for practically achievable magnetic fields, magnetohydrodynamic modification of the natural convective flow field is insignificant in high Prandtl number fluids which usually have low electrical conductivity. (For example, the electrical conductivity of a typical practical high Prandtl number fluid (e.g. heavy oil) may be of the order of 10^{-7} s/m [29]. This is in contrast to the electrical conductivity of a typical practical low Prandtl number fluid (e.g. liquid metal, ionized gas) which may be of the order of 10^6 s/m [30].) Hence, in the numerical illustrations given in the present study, we have chosen three parametric values of the Prandtl number, viz. 0.01, 0.7 and 7, typically representative of liquid metals, air and water respectively. For the vertical surface, a Prandtl number of 0.72 is considered so that direct comparison with previously published results is possible.

It is also important to understand the physical implication of the various values of \bar{x} at which results are presented. For a given fluid and fixed values of other parameters, changing values of \bar{x} represent different values of local Grashof number Gr_x . Even though Gr_x does not explicitly appear in the non-dimensional governing equations because of the particular scaling adopted, its influence on the thermo-fluid-dynamics of the convective boundary layer is critical. It is to be noted that though the temperature difference ΔT between surface and surrounding (which is primarily responsible for natural convective flow) need not be explicitly varied, it appears in the scaling velocity u_0 and, through that, in the magnetic interaction parameter M . (A related study of magnetohydrodynamic natural convection in a porous medium is given in ref. [31].)

4.1. Natural convection over a horizontal surface

The results obtained from the present computations (as functions of \bar{x} and \bar{y}) are post-processed and cast in the similarity variable form so that the existence (or non-existence) of self-similar solutions can be

Table 2

Temperature and velocity gradients at the wall for natural convection along an isothermal vertical surface ($\eta = \bar{y}/\bar{x}^{1/4}$, $\theta'(0) = d\theta/d\eta|_{\eta=0}$, $f''(0) = d^2f/d\eta^2|_{\eta=0}$).

	Present work		Similarity solution [23]		Similarity solution [7]	
	$\theta'(0)$	$f''(0)$	$\theta'(0)$	$f''(0)$	$\theta'(0)$	$f''(0)$
$Pr = 0.72, M_0 = 0$	0.5076	0.6740	0.5046	0.6760	0.5076	0.6680
$Pr = 0.72, M_0 = 1, \lambda = -1/4$	0.4506	0.5704	–	–	0.4510	0.5677
$Pr = 0.01, M_0 = 0$	0.0822	0.9881	–	–	0.0804	0.9900
$Pr = 0.01, M_0 = 1, \lambda = -1/4$	0.0723	0.7662	–	–	0.0707	0.7658

ascertained. The following similarity variables [20] are defined for the above purpose for a horizontal surface,

$$\eta = \frac{\bar{y}}{\bar{x}^{2/5}}, f'(\eta) = \frac{\bar{u}}{\bar{x}^{1/5}}, \theta(\eta) = \theta(\bar{x}, \bar{y}) \quad (31)$$

In the above expressions, η is the spatial similarity variable for the boundary layer, $f'(\eta)$ represents the dimensionless u -velocity in the boundary layer and $\theta(\eta)$ is the similarity variable for dimensionless temperature. The post-processed results are shown in Figs. 5 and 6.

For the case $\lambda = -2/5$ (for which similar solutions exist), the plots of $f'(\eta)$ (Fig. 5) and $\theta(\eta)$ (Fig. 6) at various \bar{x} -locations collapse to a single graph, as expected (this is an independent check on the accuracy of the computer program developed). However, in the case of a uniform magnetic field ($\lambda = 0$), the plots of $f'(\eta)$ and $\theta(\eta)$ versus η at various \bar{x} -locations do not superpose on one another. Fig. 5 further shows that as the downstream distance from the leading edge increases, the non-dimensional velocity profile for uniform magnetic field deviates more from the similarity velocity profile (though the rate of deviation with distance becomes small at large distance).

Fig. 7 shows the effect of an applied magnetic field on the \bar{u} -velocity at two different \bar{x} -locations along the horizontal surface and for different variations of the interaction parameter M (defined in Eq. (30) as $M_0 \bar{x}^{2\lambda}$). As a result of the damping caused by the magnetic field, the maximum of convective velocity (\bar{u}) at a particular \bar{x} -location decreases as the magnitude of M increases. The other effect of the magnetic field is that the thickness of the velocity boundary layer increases with M . It is already shown in Figs. 5 and 6 that when a uniform magnetic field is applied there is no self-similarity in the solution. Therefore, in Fig. 7, and in all subsequent figures for the horizontal case, simple non-dimensional variables such as \bar{u} , \bar{v} , θ and \bar{p} are plotted along the ordinate and simple non-dimensional distance \bar{y} is plotted as the abscissa instead of the corresponding similarity variables.

It is known that for pure natural convection [11] or for that in the presence of a magnetic field that admits self-similar solutions ($\lambda = -2/5$) [20], the maximum of the \bar{u} -velocity profile increases and shifts to greater values of \bar{y} , as \bar{x} increases. This feature is seen in the CFD solutions given in Fig. 7(a) and (b). However, it is observed that the same trend may not hold in the case of a uniform magnetic field. Fig. 7(b), for example, clearly shows that as \bar{x} increases from 5 to 10, the value of \bar{y} at which the \bar{u} -velocity attains its maxima has increased but this maximum \bar{u} -velocity has decreased. This feature, coupled with the fact that the velocity boundary layer thickness increases with increasing \bar{x} , causes the two velocity profiles to cross

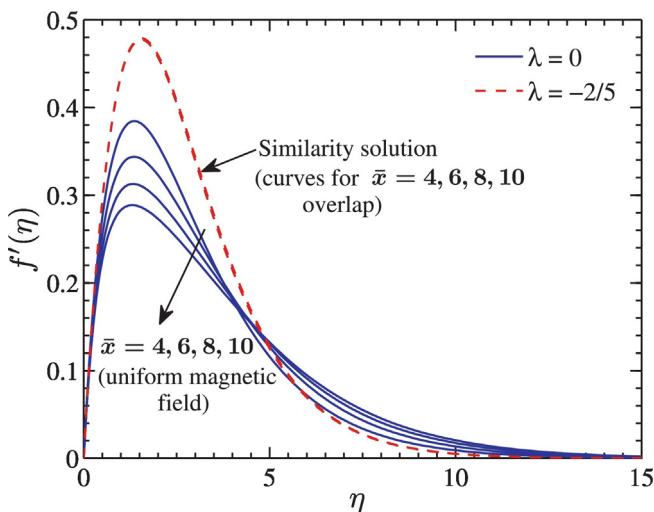


Fig. 5. CFD solution of the similarity variable representing the dimensionless u -velocity at different \bar{x} -locations along a horizontal surface for $Pr=0.7$ and $M_0=1$.

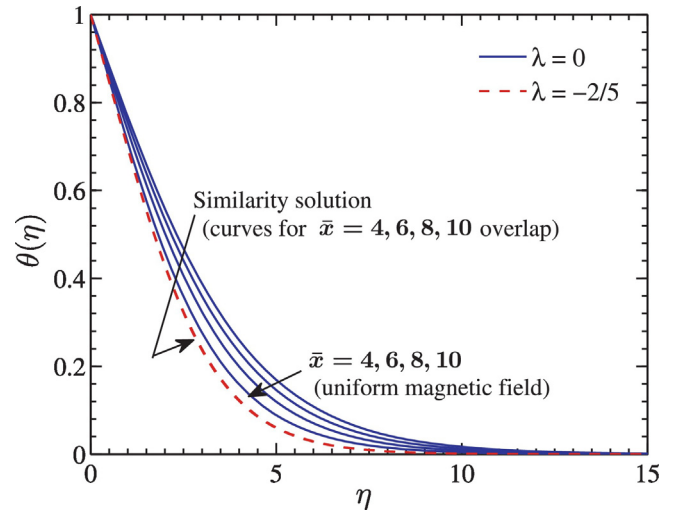


Fig. 6. CFD solution of the similarity variable representing the dimensionless temperature at different \bar{x} -locations along a horizontal surface for $Pr=0.7$ and $M_0=1$.

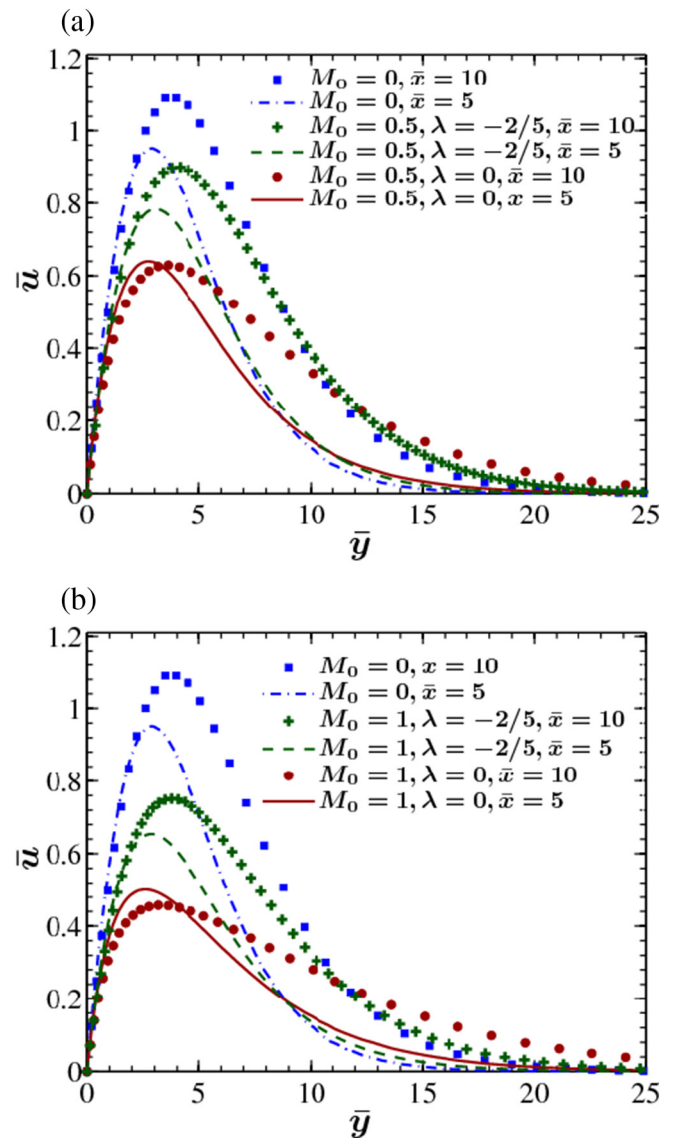


Fig. 7. Comparison of the \bar{u} profiles for $Pr=0.7$ at different \bar{x} -locations along a horizontal surface with and without magnetic field. (a) Effect of applying a vertical magnetic field with $M_0=0.5$. (b) Effect of applying a vertical magnetic field with $M_0=1$.

over. Eq. (3) shows that the Lorentz force increases linearly with the \bar{u} -velocity. This force therefore has a tendency to decelerate the faster moving fluid to a greater extent as compared to the slower moving fluid (i.e. the Lorentz force affects the peak of the \bar{u} -velocity profile more than its tail). This tendency plays a role in the crossing-over of the velocity profiles as observed for the uniform field. In order to understand why the crossing-over is not observed for the case of $\lambda = -2/5$, it is to be realized that, for the case of $\lambda = -2/5$, the intensity of the magnetic field and hence the damping force it generates, decreases along \bar{x} (as an example, at $\bar{x} = 10$, $M = 0.16M_0$). The Lorentz force still decreases the rate of increase of \bar{u} with \bar{x} , the increase being an inherent trend in pure natural convection, but is unable to reverse the trend.

Figs. 8–11 represent CFD solutions for the flow of a low Prandtl number fluid on horizontal surfaces with M_0 as a parameter. Fig. 8 shows that, as M_0 increases, the maximum u -velocity decreases and the thickness of the boundary layer increases. The \bar{y} -location at which the maximum velocity occurs also shifts towards the surface as M_0 increases. Thus the \bar{u} -velocity profiles gradually flatten as M_0 is increased. A comparison of Figs. 7 and 8 reveals that, at low values of Pr , the velocity profiles become pointed near the maxima with the velocity dropping off rapidly on both sides of the maxima. The thicknesses of both velocity and thermal boundary layers become considerably greater as the Prandtl number decreases.

Fig. 9 shows the \bar{v} -velocity profiles inside the boundary layer on a horizontal surface for different values of M_0 . The \bar{v} -velocity changes sign inside the boundary layer, being positive near the surface and then becoming negative when \bar{y} exceeds a certain value. So, the overall flow may be visualized as two streams, one stream appearing to rise from the isothermal surface and the other stream descending from the surrounding fluid present just outside the boundary layer. The two streams interact at some \bar{y} -location (where $\bar{v} = 0$) which is not very far away from the surface. As $\bar{y} \rightarrow \infty$, the entrainment velocity from the surrounding, whose magnitude decreases with increasing intensity of the applied magnetic field. The magnitude of \bar{v} -velocity close to the isothermal surface increases with increasing M_0 ; however, the magnitude decreases with increasing M_0 after a certain distance from the surface. This reversal in trend is due to the change of sign of the \bar{v} -velocity.

A study of Eqs. (4) and (5) shows that the variation of \bar{v} -velocity follows a first order equation in \bar{y} ; hence, only one mathematical boundary

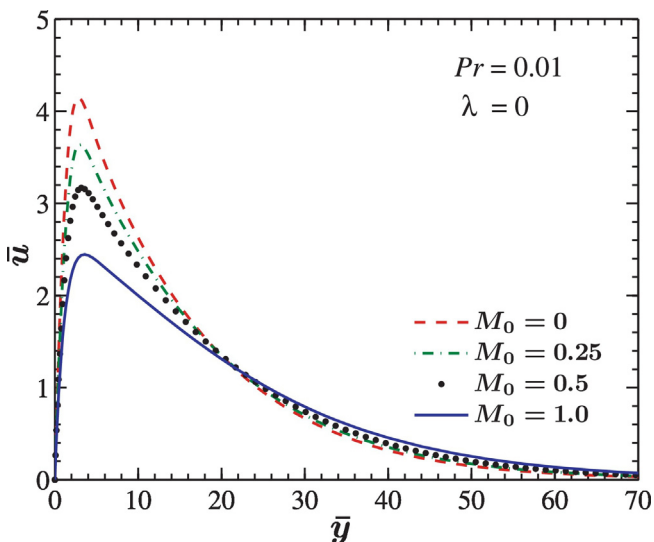


Fig. 8. CFD solution for the variation of \bar{u} -velocity in a low Prandtl number fluid at $\bar{x} = 5$ on a horizontal surface with varying strength of a uniform magnetic field. [The \bar{y} axis is shown here up to a value of 70 for clarity of the graphs, the maximum value used in the computations is greater so as to ensure \bar{u} asymptotically approaches zero.]

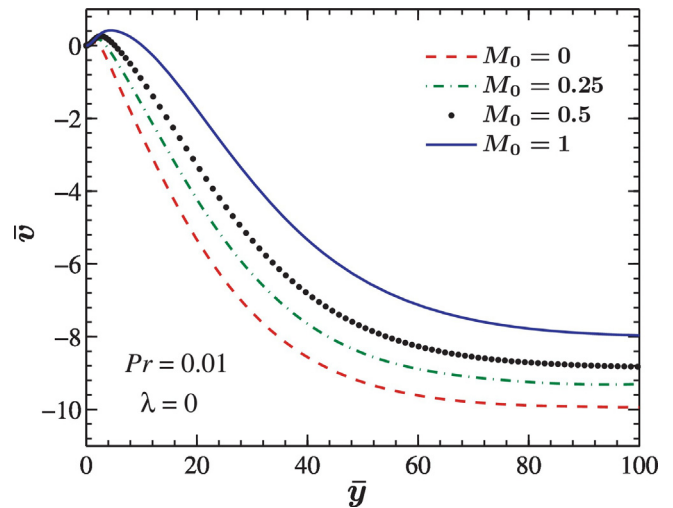


Fig. 9. CFD solution for variation of the \bar{v} -velocity in a low Prandtl number fluid at $\bar{x} = 5$ on a horizontal surface with varying strength of a uniform magnetic field.

condition is needed, which is provided on the solid surface, i.e. at $\bar{y} \rightarrow 0$ (no penetration through an impervious wall). Since the \bar{u} -velocity is zero everywhere in the region of the computational domain that lies outside the boundary layer, the value of $\partial \bar{u} / \partial \bar{x}$ is zero there. From the continuity equation (Eq. (4)) it follows that $\partial \bar{v} / \partial \bar{y}$ should also be zero there, indicating that \bar{v} attains a constant value at the edge of the boundary layer. This value evolves from the solution of the equations itself. The entrainment velocity at $\bar{y} \rightarrow \infty$ is, therefore, not prescribed but automatically calculated by the CFD program. The importance of providing a sufficiently large computational domain in the \bar{y} -direction, so that all flow variables asymptotically approach their respective values at $\bar{y} \rightarrow \infty$, was mentioned in Section 3.2. This is of the greatest importance in the computation of \bar{v} , for which (unlike the other flow variables) no mathematical boundary condition is imposed at $\bar{y} \rightarrow \infty$, and the final solution must evolve such that the correct, finite entrainment velocity is obtained there.

The non-dimensional temperature (θ) distribution inside the boundary layer on a horizontal surface for different values of M_0 is shown in Fig. 10. As M_0 increases, the temperature of the fluid at a particular \bar{y} -location increases. This is a direct outcome of the reduced convective flow velocity which results in less amount of heat being carried

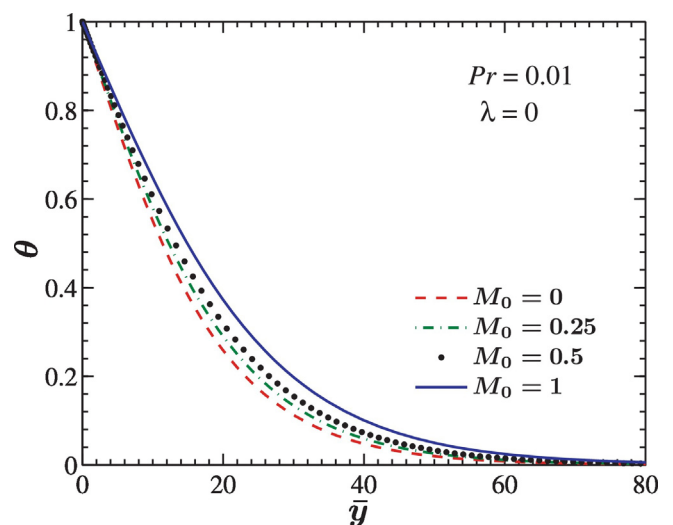


Fig. 10. CFD solution for variation of the dimensionless temperature in a low Prandtl number fluid at $\bar{x} = 5$ on a horizontal surface with varying strength of a uniform magnetic field.

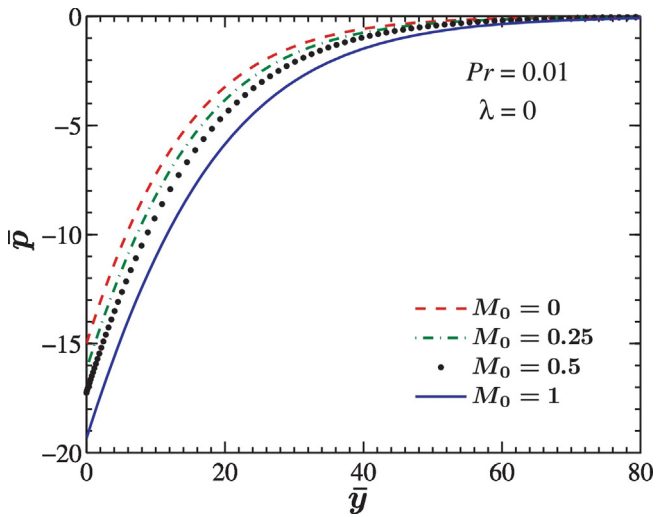


Fig. 11. CFD solution for variation of the dimensionless static pressure in a low Prandtl number fluid at $\bar{x} = 5$ on a horizontal surface with varying strength of a uniform magnetic field.

away from the hot surface. It is found in Fig. 9 that the value of \bar{y} at which \bar{v} changes sign, increases with increase in M_0 . This indicates that the fluid stream appearing to rise from the heated isothermal surface meets the descending stream at progressively increasing distances from the solid surface as M_0 increases. Such a phenomenon may be attributed to the increased temperature of the fluid near the solid surface with increasing M_0 . Fig. 11 shows that the non-dimensional pressure \bar{p} inside the natural convective boundary layer increases from a negative value at the surface to reach zero asymptotically at the edge of the boundary layer. The magnitude of \bar{p} at $\bar{y} = 0$ increases with an increase in M_0 .

The effects of the variation of M and Pr on the reduced Nusselt number Nu^* ($-\partial\theta/\partial\bar{y}|_{\bar{y}=0}$) and the reduced skin-friction coefficient c_f^* ($(\partial\bar{u}/\partial\bar{y})|_{\bar{y}=0}$) are given in Table 3. Following the same trend as in pure natural convection, as Pr is increased, Nu^* increases and c_f^* decreases in magnetohydrodynamic natural convection too. It is observed that for the case of a uniform magnetic field, as M_0 is increased, both Nu^* and c_f^* decreases. This may be attributed to the reduced convective velocities with increasing M_0 and the associated increase in the temperature near the surface, which result in decreased velocity and temperature gradients there. Table 3 further shows that for a fixed value of Pr and M_0 , the values of Nu^* and c_f^* for $\lambda = 0$ are significantly different from those for $\lambda = -2/5$.

Table 3
Variation of the reduced Nusselt number and the reduced skin-friction coefficient at $\bar{x} = 10$ for a horizontal surface.

Pr	M_0	λ	Nu^*	c_f^*
0.01	0	0	0.0348	2.8156
	0.25	0	0.0314	2.2329
	0.50	0	0.0276	2.0187
	1.00	0	0.0220	1.7890
	1.00	-2/5	0.0315	2.0755
0.7	0	0	0.1430	0.6205
	0.25	0	0.1248	0.5272
	0.50	0	0.1108	0.5027
	1.00	0	0.0933	0.4500
	1.00	-2/5	0.1188	0.4779
7	0	0	0.2488	0.2599
	0.25	0	0.2274	0.2468
	0.50	0	0.2053	0.2397
	1.00	0	0.1862	0.2276
	1.00	-2/5	0.2286	0.2129

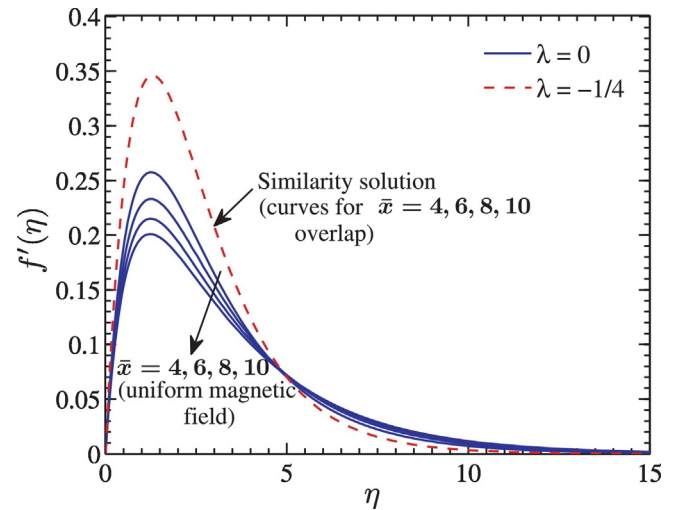


Fig. 12. CFD solution of the similarity variable representing the dimensionless u -velocity at different \bar{x} -locations along a vertical surface for $Pr = 0.72$ and $M_0 = 1$.

4.2. Natural convection past a vertical surface

For a vertical surface, the computational results, obtained as functions of \bar{x} and \bar{y} , are post-processed and recast in terms of the following similarity variables [6]:

$$\eta = \frac{\bar{y}}{\bar{x}^{1/4}}, f'(\eta) = \frac{\bar{u}}{\bar{x}^{1/2}}, \theta(\eta) = \theta(\bar{x}, \bar{y}) \quad (32)$$

The similarity variables $f'(\eta)$ and $\theta(\eta)$ are plotted against η in Figs. 12 and 13 respectively. The CFD program accurately produces self-similar solution, when it exists (i.e., when $\lambda = -1/4$ [6,7]). When a uniform magnetic field ($\lambda = 0$) is applied the plots of $f'(\eta)$ and $\theta(\eta)$ versus η at different \bar{x} -locations do not collapse to a single graph, thus demonstrating the non-existence of self-similar solution.

Fig. 14 shows the effect of an applied magnetic field on the \bar{u} -velocity at two \bar{x} -locations along the vertical surface and for different variations of the interaction parameter M . Some of the features of the convective flow past the vertical surface, observable in Fig. 14, are similar to those seen in Fig. 7 for the horizontal surface. These include, the reduction of \bar{u} -velocity and the thickening of the boundary layer at a particular \bar{x} -location with increasing M , and, the smaller convective velocities and thicker boundary layers for the uniform magnetic field as compared to the field that admits self-similar solutions ($\lambda = -1/4$) for the same value of M_0 .

As in the case of a horizontal surface, the maxima of the \bar{u} -velocity profiles for pure natural convection past a vertical surface or for that in the presence of a magnetic field with $\lambda = -1/4$, increase in magnitude and shift to greater values of \bar{y} , as \bar{x} increases. The same behaviour of the maxima of the \bar{u} -velocity profiles is observed even for a uniform magnetic field, which is unlike what happens for a horizontal surface. However, it is observed in Fig. 14(a) and (b) that as the value of M_0 increases (for $\lambda = 0$), the gap between the \bar{u} -velocity profiles at $\bar{x} = 5$ and $\bar{x} = 10$ decreases. Hence it is possible that for values of M higher than what has been investigated here (i.e. for $M > 1$), the vertical surface may also show features similar to those seen in Fig. 7.

Fig. 15 shows the effects of altering the uniform magnetic field (by varying M_0) when the Prandtl number of the fluid is low. The results are shown at $\bar{x} = 5$. A comparison of Figs. 14 and 15 reveals that, at low values of Pr , the velocity profiles become pointed near the maxima with the velocity dropping off rapidly on both sides of the maxima. The thicknesses of both velocity and thermal boundary layers become considerably greater as the Prandtl number decreases.

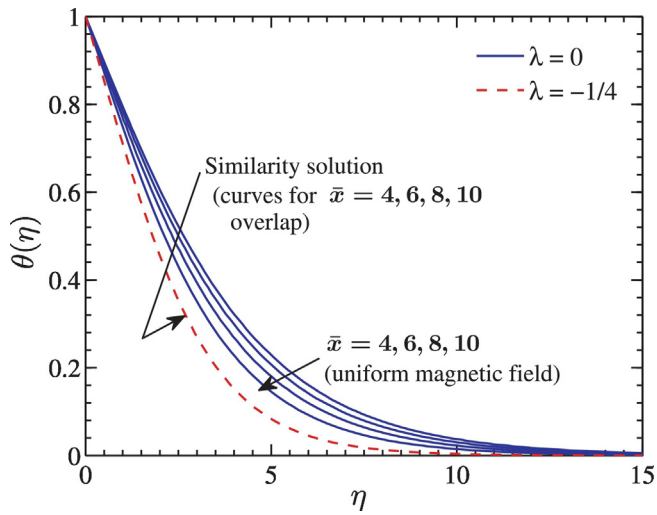


Fig. 13. CFD solution of the similarity variable representing the dimensionless temperature at different \bar{x} -locations along a vertical surface for $Pr=0.72$ and $M_0=1$.

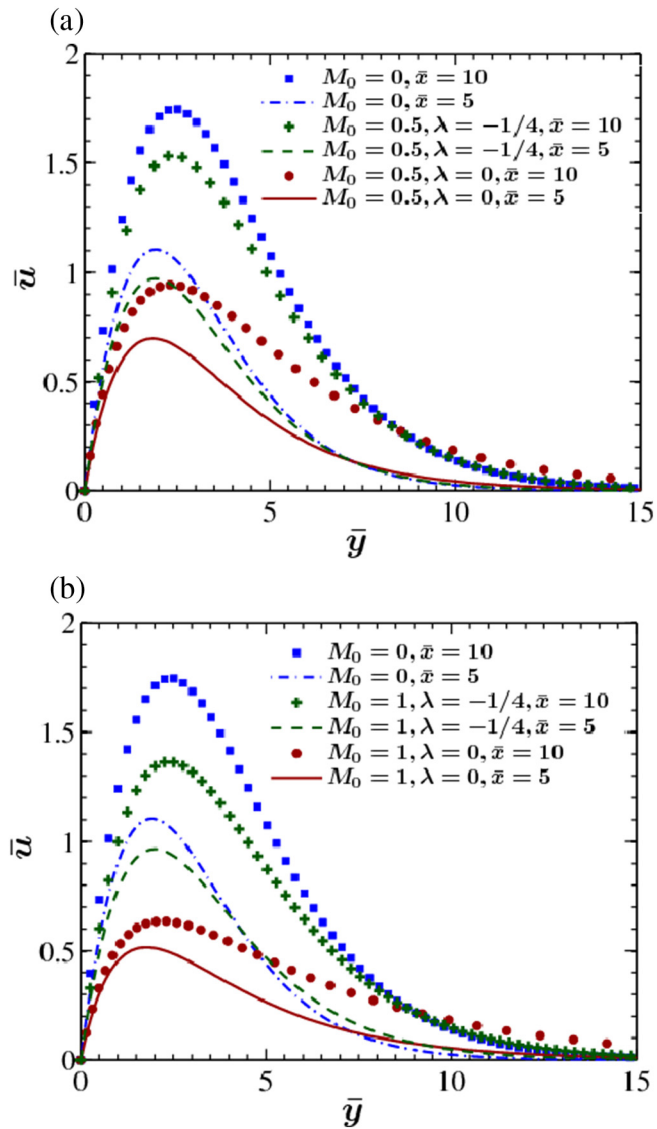


Fig. 14. Comparison of the \bar{u} profiles for $Pr=0.72$ at different \bar{x} -locations along a vertical surface with and without magnetic field. (a) Effect of applying a horizontal magnetic field with $M_0=0.5$. (b) Effect of applying a horizontal magnetic field with $M_0=1$.

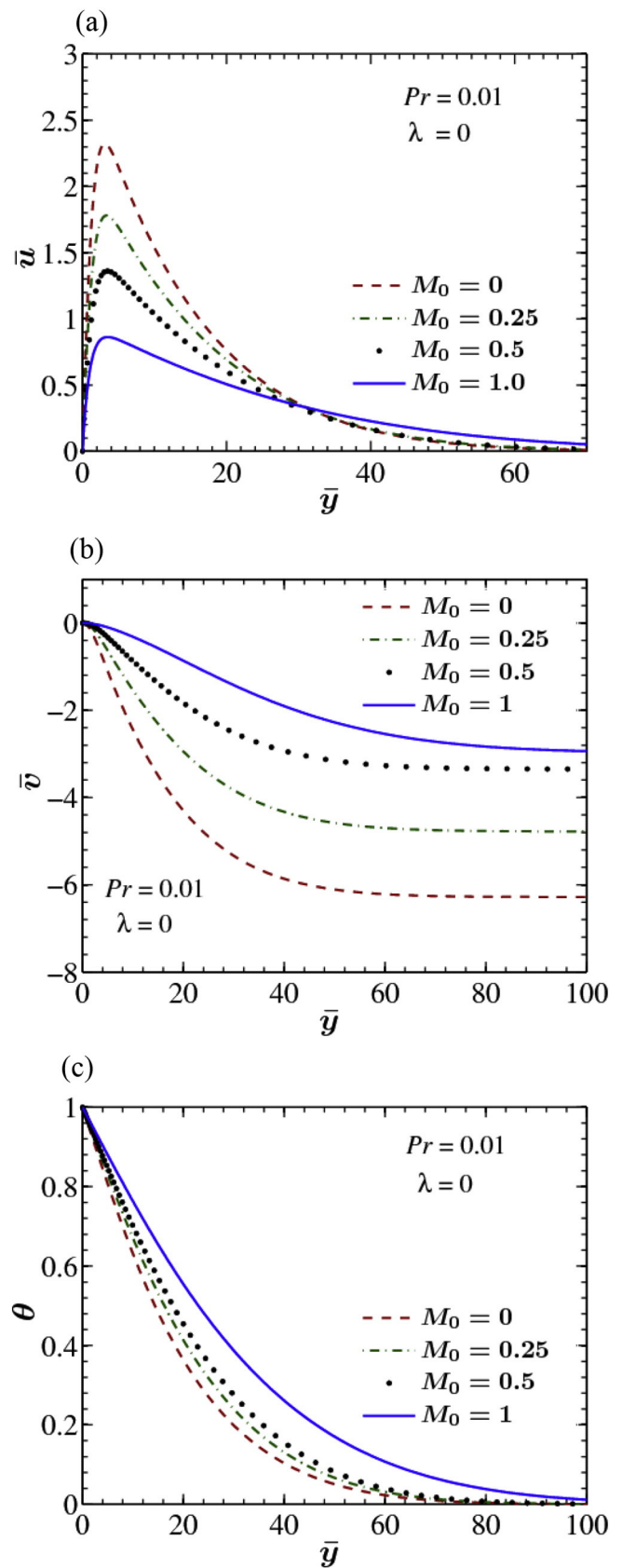


Fig. 15. CFD solution for natural convection in a low Prandtl number fluid along a vertical surface at $\bar{x}=5$ for varying strength of a uniform magnetic field. (a) Variation of \bar{u} -velocity, (b) variation of \bar{v} -velocity and (c) variation of temperature.

A comparison of Figs. 8 and 15(a), and that of Figs. 10 and 15(c) show that the same value of M_0 seem to produce more pronounced effect on the u -velocity and temperature profiles for the vertical case than those for the horizontal case. This is because of the fact that for the same value of M_0 (calculated from Eqs. (10) and (19)), the strengths of the applied magnetic field for the horizontal case ($B_{horizontal}$) and the vertical case ($B_{vertical}$) are related by the Grashof number according to the relation $B_{vertical}/B_{horizontal} = Gr_L^{1/20}$ (which is greater than 1 for $Gr_L \geq 1000$).

A comparison of Figs. 9 and 15(b) reveals the similarities and differences, in the variation of \bar{v} -velocity, between the horizontal and vertical surfaces. Like the horizontal case, the entrainment velocity $\bar{v}|_{\bar{y} \rightarrow \infty}$ is not prescribed but automatically calculated by the CFD program for the vertical case. Since $\partial \bar{u} / \partial \bar{x}$ is zero outside the boundary layer, it follows from Eq. (14) that $\partial \bar{v} / \partial \bar{y}$ should also be zero there, indicating that \bar{v} attains a constant value (the entrainment velocity) at the edge of the boundary layer. This value evolves from the solution of the equations itself. However, unlike the horizontal case, there is no change in the sign of \bar{v} -velocity for the case of vertical surface and the value of \bar{v} is negative everywhere within the boundary layer. At any given \bar{x} and \bar{y} , the magnitude of \bar{v} decreases either with increasing M_0 or increasing Pr .

Table 4 shows that the variations with Pr and M_0 of the reduced Nusselt number Nu^* and the reduced skin-friction coefficient c_f^* follow the same trends for natural convection past a vertical surface as they were found for the horizontal surface. Table 4 further shows that for a fixed value of Pr and M_0 , the values of Nu^* and c_f^* for $\lambda = 0$ are significantly different from those for $\lambda = -1/4$. Hence it would not be appropriate to predict the effect of a uniform magnetic field from the existing similarities solutions.

4.3. Spatial evolution of the convective velocity profiles

An interesting feature of magnetohydrodynamic natural convection may be appreciated by comparing Figs. 7 and 14. For the vertical surface (Fig. 14), it is found that as \bar{x} increases, the maximum value of \bar{u} increases. The same trend is obtained in simple natural convection (i.e. in the absence of a magnetic field) for either a vertical or horizontal surface. Fig. 7 shows that the same feature is retained also for a horizontal surface for a specific variation of the magnetic field along the surface ($B \propto \bar{x}^{-2/5}$). However, when a uniform magnetic field is applied (for either $M_0 = 0.5$ or $M_0 = 1.0$), Fig. 7 shows that the maximum of \bar{u} at $\bar{x} = 1$ 0 is smaller than the maximum of \bar{u} at $\bar{x} = 5$. This suggests that the natural increase of the maximum of \bar{u} -velocity with \bar{x} due to pure natural convection, is exceeded by the decrease due to the damping action of the magnetic field. This situation, depicted in Fig. 7, makes one uneasy since the question arises whether the natural convective flow may

Table 4
Variation of the reduced Nusselt number and the reduced skin-friction coefficient at $\bar{x} = 10$ for a vertical surface.

Pr	M_0	λ	Nu^*	c_f^*
0.01	0	0	0.0327	1.2425
	0.25	0	0.0260	1.1361
	0.50	0	0.0213	0.8954
	1.00	0	0.0180	0.7588
	1.00	-1/4	0.0251	0.9635
0.72	0	0	0.2018	0.8475
	0.25	0	0.1724	0.7822
	0.50	0	0.1584	0.7186
	1.00	0	0.1345	0.6043
	1.00	-1/4	0.1653	0.7172
7	0	0	0.4361	0.7599
	0.25	0	0.3853	0.6464
	0.50	0	0.3536	0.5778
	1.00	0	0.3196	0.4866
	1.00	-1/4	0.3775	0.6195

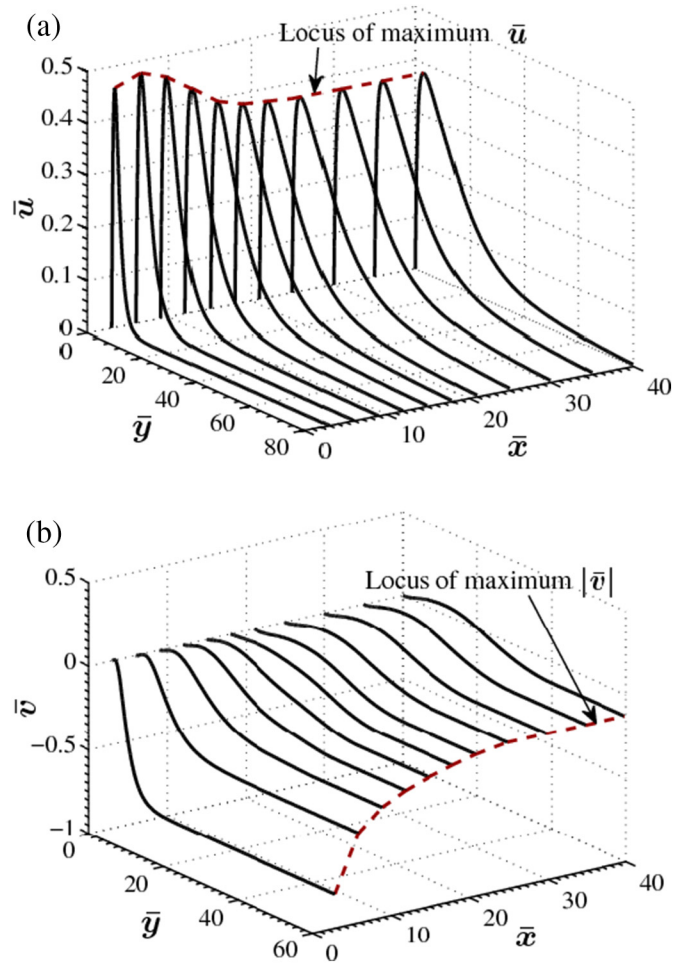


Fig. 16. Predictions of the present theory showing the evolution of the \bar{u} -velocity and \bar{v} -velocity along the horizontal surface for a uniform magnetic field with $M_0 = 1$ and $Pr = 0.7$. (a) \bar{u} -velocity and (b) \bar{v} -velocity.

stop altogether at a sufficiently large value of \bar{x} . In order to shed further light on this issue, computations for a uniform magnetic field with $M_0 = 1.0$ ($Pr = 0.7$) are continued up to a large value of \bar{x} ($\bar{x}_{max} = 40$). The spatial evolution of the profiles of \bar{u} and \bar{v} are shown respectively in Fig. 16(a) and (b). Profiles are drawn at a few selected \bar{x} locations only so that the figures are not crammed. The locus of maxima given in Fig. 16(a) shows that, when the applied magnetic field is uniform, for a horizontal surface, the maximum of \bar{u} at first increases with an increase in \bar{x} but then decreases with any further increase in \bar{x} . At large \bar{x} , the maximum of \bar{u} velocity tends to approach a constant value asymptotically instead of continuously decreasing to a vanishing magnitude. The boundary layer thickness, however, continuously increases with increasing \bar{x} . Fig. 16(b) shows that the maximum of $|\bar{v}|$ (i.e. the magnitude of the entrainment velocity) decreases continuously with increasing \bar{x} , though the rate of decrease diminishes with increasing \bar{x} .

Fig. 14 (vertical surface) shows that the maximum values of \bar{u} -velocity follow the same trend as in pure natural convection. However, the decrease in the difference between the maximum values for two values of \bar{x} with an increase in M_0 indicates that for values of M higher than what has been investigated here (i.e. for $M > 1$), the vertical surface may also show the above-mentioned evolutionary features of the horizontal surface.

4.4. A final look at similarity analysis versus present CFD simulations

An inspection of Tables 3 and 4 shows that considerable differences exist between the solutions for a uniform magnetic field and the

Table 5Relative difference in Nusselt number, $\Delta \hat{Nu}$ given by Eq. (33) ($\bar{x} = 10, M_0 = 1$).

Configuration	$Pr = 0.01$	$Pr = 0.7$	$Pr = 7$
Horizontal	43.18%	27.33%	22.77%
Vertical	39.44%	22.90%	18.12%

similarity solutions valid for the restrictive assumptions on the variation of the magnetic field ($B \propto \bar{x}^{-1/4}$ for a vertical surface and $B \propto \bar{x}^{-2/5}$ for a horizontal surface). This difference becomes more prominent at a low value of Prandtl number. The relative difference in the value of the Nusselt number, $\Delta \hat{Nu}$, is defined as

$$\Delta \hat{Nu} = \frac{Nu_{similarity}^* - Nu_{uniform}^*}{Nu_{uniform}^*} \quad (33)$$

In Eq. (33), the subscript 'similarity' refers to the case of a magnetic field which admits similarity solution and the subscript 'uniform' refers to the case of a uniform magnetic field. Sample values of $\Delta \hat{Nu}$ are given in Table 5. It is clear that the results of the similarity theory cannot be used if the magnetic field is uniform in a practical situation. Herein lies the importance of the present computations.

It is to be appreciated that the developed numerical scheme can accommodate any arbitrary variation of the magnetic field even though example calculations are presented for two situations: (i) the case of a uniform magnetic field (which represents the most practical situation) and (ii) variable magnetic fields which admit self-similarity.

5. Conclusion

A time-marching finite difference technique is used to obtain the steady-state solutions for magnetohydrodynamic natural convection adjacent to heated horizontal as well as vertical surfaces. This has allowed us to establish overall similarities and several subtle differences between the two cases (Section 4). The computer program has been so developed that it is possible to study the effect of any arbitrary variation of the applied magnetic field. The CFD solutions obtained by the present method, for a power-law variation of the magnetic field $B = B_0 \bar{x}^\lambda$, are found to be in excellent agreement with the results predicted by similarity theory. However, the practical utility of such restrictively variable magnetic fields ($\lambda = -2/5$ or $\lambda = -1/4$) is questionable. In the example calculations of the present work, particular attention is paid to the case of uniform magnetic field which perhaps bears the greatest practical significance (but cannot be solved by the similarity transformation method).

The damping force generated by a magnetic field reduces the convective flow velocity (u). This reduced velocity results in less heat being carried away from the heated surface and a consequent increase in the fluid temperature adjacent to the surface. The mutual interaction of two effects, viz. the increase of the maximum of \bar{u} -velocity with \bar{x} in any natural convective flow and the damping action of a magnetic field, results in complex variations of the maximum of \bar{u} -velocity with \bar{x} . The magnitude of the non-dimensional entrainment velocity $\bar{v}|_{\bar{y} \rightarrow \infty}$, which is not prescribed but automatically calculated by the CFD program, is found to decrease with an increase in any of the three important parameters, viz. Gr_x , Pr and M_0 . It is established here that, for a successful, accurate CFD simulation of natural convective boundary layer flow, the \bar{y} -extent of the computational domain needs to be appropriately adjusted with the variation of \bar{x} (i.e. Gr_x), Pr and M_0 , so that all flow variables asymptotically approach their respective values at large \bar{y} .

The reduced Nusselt number Nu^* increases and the reduced skin-friction coefficient c_f^* decreases with an increase in Pr . For a uniform magnetic field, both Nu^* and c_f^* decrease with an increase in M_0 . For

the same value of M_0 , both Nu^* and c_f^* are significantly smaller for $\lambda = 0$ than those for values of λ which admit self-similar solutions. Thus, if simulating the effect of a uniform magnetic field is the computational objective from practical considerations, then the existing similarity solutions are poor substitutes for a full CFD solution such as the present study.

Acknowledgements

The authors express their appreciation to L. Agarwal, a former BTech project student of Prof. Guha, who worked on magnetohydrodynamic natural convection.

References

- [1] P.A. Davidson, *An Introduction to Magnetohydrodynamics*, first ed. Cambridge University Press, Cambridge, UK, 2001.
- [2] G. Sposito, M. Ciofalo, One-dimensional mixed MHD convection, *Int. J. Heat Mass Transf.* 49 (17–18) (2006) 2939–2949.
- [3] A. Ishak, R. Nazar, I. Pop, MHD mixed convection boundary layer flow towards a stretching vertical surface with constant wall temperature, *Int. J. Heat Mass Transf.* 53 (23–24) (2010) 5330–5334.
- [4] N. Riley, Magnetohydrodynamic free convection, *J. Fluid Mech.* 18 (4) (1964) 577–586.
- [5] A.S. Gupta, Steady and transient free convection of an electrically conducting fluid from a vertical plate in the presence of a magnetic field, *Appl. Sci. Res.* 9 (1) (1960) 319–333.
- [6] P.S. Lykoudis, Natural convection of an electrically conducting fluid in the presence of a magnetic field, *Int. J. Heat Mass Transf.* 5 (1–2) (1962) 23–34.
- [7] E.M. Sparrow, R.D. Cess, The effect of a magnetic field on free convection heat transfer, *Int. J. Heat Mass Transf.* 3 (4) (1961) 267–274.
- [8] H. Schlichting, K. Gersten, *Boundary Layer Theory*, eighth ed. Springer, New Delhi, India, 2004.
- [9] A. Guha, S. Samanta, Closed-form analytical solutions for laminar natural convection on horizontal plates, *J. Heat Transfer* 135 (10) (2013) 1–9, 102501.
- [10] Z. Rotem, L. Claassen, Natural convection above unconfined horizontal surfaces, *J. Fluid Mech.* 39 (1) (1969) 173–192.
- [11] S. Samanta, A. Guha, A similarity theory for natural convection from a horizontal plate for prescribed heat flux or wall temperature, *Int. J. Heat Mass Transf.* 55 (13–14) (2012) 3857–3868.
- [12] A. Guha, K. Pradhan, Natural convection of non-Newtonian power-law fluids on a horizontal plate, *Int. J. Heat Mass Transf.* 70 (2014) 930–938.
- [13] K. Pradhan, S. Samanta, A. Guha, Natural convective boundary layer flow of nanofluids above an isothermal horizontal plate, *J. Heat Transfer* 136 (10) (2014) 1–8, 102501.
- [14] A. Guha, K. Pradhan, A unified integral theory of laminar natural convection over surfaces at arbitrary inclination from horizontal to vertical, *Int. J. Therm. Sci.* 111 (2017) 475–490.
- [15] A. Guha, S. Sengupta, Effects of finiteness on the thermo-fluid-dynamics of natural convection above horizontal plates, *Phys. Fluids* 28 (6) (2016) 1–29, 063603.
- [16] A.S. Gupta, Hydromagnetic free convection flows from a horizontal plate, *AIAA J.* 4 (8) (1966) 1439–1441.
- [17] P. Singh, Hydromagnetic free convection flow from a horizontal plate: non-similar solutions, *Acta Physiol. Acad. Sci. Hung.* 34 (1) (1973) 1–11.
- [18] P. Singh, Hydromagnetic free convection flow from a horizontal plate: similar solutions, *Acta Physiol. Acad. Sci. Hung.* 38 (2) (1975) 109–116.
- [19] S.N. Singh, C.J. Cremers, Magnetohydrodynamic free convection from a horizontal plate, *Phys. Fluids* 12 (2) (1969) 379–380.
- [20] S. Samanta, A. Guha, Magnetohydrodynamic free convection flow above an isothermal horizontal plate, *Commun. Nonlinear Sci. Numer. Simul.* 18 (12) (2013) 3407–3422.
- [21] I.E. Sarris, G.K. Zikos, A.P. Grecos, N.S. Vlachos, On the limits of validity of the low magnetic Reynolds number approximation in MHD natural-convection heat transfer, *Numer. Heat Transfer, Part B* 50 (2) (2006) 157–180.
- [22] K. Stewartson, On the free convection from a horizontal plate, *Z. Angew. Math. Phys.* 9 (3) (1958) 276–282.
- [23] L.C. Burmeister, *Convective Heat Transfer*, second ed. John Wiley and Sons, New York, USA, 1993.
- [24] E.M. Sparrow, Laminar free convection on a vertical plate with prescribed nonuniform wall heat flux or prescribed nonuniform wall temperature, *NACA TN-3508*, 1955.
- [25] A. Guha, J.B. Young, Time-marching prediction of unsteady condensation phenomena due to supercritical heat addition, *Turbomachinery: Latest Developments in a Changing Scene*, Institution of Mechanical Engineers, London, UK, 1991 (ISBN 0852987617).
- [26] A. Guha, Thermal choking due to nonequilibrium condensation, *J. Fluids Eng.* 116 (3) (1994) 599–604.
- [27] Y. Mei, A. Guha, Implicit numerical simulation of transonic flow through turbine cascades on unstructured grids, *Proc. Inst. Mech. Eng. A J. Power Energy* 219 (1) (2005) 35–47.
- [28] A. Guha, S. Samanta, Effect of thermophoresis and its mathematical models on the transport and deposition of aerosol particles in natural convective flow on vertical and horizontal plates, *J. Aerosol Sci.* 77 (2014) 85–101.
- [29] S. Mannan, F.P. Lees, *Lees' Loss Prevention in the Process Industries: Hazard Identification, Assessment and Control*, second ed. Elsevier Butterworth-Heinemann, USA, 2005.
- [30] J. Blizt, *Electrical and Magnetic Methods of Non-destructive Testing*, Adam Hilger imprint by IOP Publishing Ltd., Bristol, England, 1991.
- [31] K. Pradhan, A. Guha, Natural convection above a horizontal plate in a nanofluid-saturated porous medium with or without a magnetic field, *J. Porous Med.* 18 (6) (2015) 613–628.